ADVANCED ENERGY MATERIALS
www.advenergymat.de

A Three-Terminal Hybrid Thermionic-Photovoltaic Energy Converter

Alessandro Bellucci, Pablo García-Linares, Antonio Martí, Daniele Maria Trucchi, and Alejandro Datas**

Hybrid thermionic-photovoltaics (TIPV) are solid-state thermal-to-electric energy converters that rely on the non-isothermal transport of photons and electrons through a vacuum gap. In contrast to pure thermionic converters, the absorption of photons in a photovoltaic anode produces an electrochemical potential that can be delivered as electricity, ultimately boosting the power generation capacity of the device. In this work, the proof of concept of a three-terminal TIPV converter where thermionic and photogenerated currents are collected independently is reported. Thermionic electrons are injected in the conduction band of a semiconducting anode (n-type InP), from where they are directly extracted. Photogenerated electrons are also extracted from the conduction band of the anode, but they are then reinjected in the valence band through an independent hole-selective contact (p-type InGaAs). By using a low workfunction engineered anode (BaF_x/InP) and cathode (Sc_xO_y/W) a maximum power generation capacity of 125.6 and 0.35 mW cm^{-2} for PV and thermionic sub-devices, respectively, is demonstrated, operating at 1400 °C. This proof of concept paves the way for the development of efficient hybrid thermionic and photovoltaic converters for the direct conversion of heat into electricity, and subsequently contributes to finding an efficient alternative to thermoelectric generators.

1. Introduction

Thermophotovoltaics (TPV)[1,2] and thermionic energy converters (TECs)[3] are highly efficient and high temperature alternatives to thermoelectrics[4] that rely on the non-isothermal transport of fundamental particles (photons for TPV and electrons for TEC) through space. Unlike thermoelectrics, the lack of solid continuity between the hot and cold side of the device confers both TPV and TEC the ability to operate at higher temperature gradients with minimal parasitic internal heat loss, theoretically enabling higher conversion efficiencies. As a matter of fact, TPV cells made of low bandgap energy semiconductors like $In_{0.53}Ga_{0.47}As$ ($E_g \approx 0.75$ eV) have recently demonstrated conversion efficiencies around 30% at hot-side temperatures of ≈1200 °C.[5,6] On the other hand, current TECs have reported efficiencies only slightly above 10% at hot-side temperatures above 1000 °C,[3] which is still in the range of thermoelectric generators.[7] Possible solutions to increase the conversion efficiency of TEC include i) the development of ultra-low work function coatings for the cathode and the anode and ii) the establishment of micro-scale vacuum gaps that prevent the accumulation of electrons within the gap and thus, avoid the formation of an electric field that opposes the flow of electrons (the so-called "space charge effect"). The interelectrode distance that is needed to fully eliminate the space charge decreases with the thermionic current, and distances lower than 1 µm may be needed to reach high TEC power densities.[8] However, at such small interelectrode distances, near-field radiation (tunneling of evanescent waves between the cathode and the anode) significantly contributes to the energy transfer and represents a significant source of heat loss. Therefore, the selection of the interelectrode distance in a conventional TEC must fulfill a trade-off that minimizes both space charge and thermal radiation losses to result in the highest conversion efficiency.[8]

Hybrid thermionic-photovoltaic (TIPV) converters have been recently proposed as a means to harvest both electrons and photons emitted from high temperature sources.[9] In this device, thermal radiation is no longer wasted but is converted into electricity. Thus, interelectrode distances as low as technically feasible could be implemented.[10,11] Two different TIPV device configurations have been proposed so far: two-terminal and three-terminal. In two-terminal TIPV devices, thermionic electrons emitted by a hot emitter (the cathode) are injected in the valence band of a semiconducting collector (the anode), then pumped to the conduction band by the photovoltaic (PV)

A. Bellucci, D. M. Trucchi
Istituto di Struttura della Materia
DiaTHEMA Lab, Sez. Montelibretti
Consiglio Nazionale delle Ricerche
Via Salaria, km 29.300, Monterotondo (RM) 00015, Italy
E-mail: alessandro.bellucci@cnr.it
P. García-Linares, A. Martí, A. Datas
Instituto de Energía Solar
Universidad Politécnica de Madrid
Avenida Complutense, 30, Madrid 28040, Spain
E-mail: a.datas@upm.es
The ORCID identification number(s) for the author(s) of this article can be found under https://doi.org/10.1002/aenm.202200357.

DOI: 10.1002/aenm.202200357

effect and finally extracted from the conduction band to produce useful energy before they are reinjected in the cathode. The proof of concept experiment of a two terminal TIPV device has been recently reported using a high-temperature polycrystalline tungsten cathode and both GaAs[12] and InGaAs PV anodes,[13] demonstrating a higher output voltage and power generation capacity than a baseline thermionic converter that uses the same materials.

The two-terminal TIPV device configuration described above faces two main limitations: first, the rate of thermionic and photogenerated electrons must be equal, that is, the thermionic and PV sub-devices are internally connected in series, and thus, the sub-device producing a higher current will be biased near open-circuit conditions rather than at its maximum power point. The unique current, flowing throughout the whole device, imposes a demanding condition that is only met at a particular cathode temperature or interelectrode separation distance,[10,11] making its efficiency very sensitive to both variables. Second, the two-terminal configuration requires thermionic electrons to be injected in the valence band of the semiconducting anode and this requires the anode' surface to be a hole-selective contact for the carriers photogenerated within the semiconductor. Hole-selective contacts (e.g., p-type semiconductor) have the Fermi energy level pinned near the valence band, and thus, they usually have higher work functions than their electron-selective counterparts (e.g., n-type semiconductor). Therefore, the resultant TIPV device may be penalized with a lower thermionic voltage contribution.

These two-terminal TIPV configuration drawbacks can be solved using a three-terminal architecture, with the n-type contact of the PV cell facing the emitter, thus, inverting the position of the p-n junction, as it is shown in **Figures 1**a, **2**. Because an n-type collector is used in this case, the Fermi energy level is pinned near the conduction band. Thus, a lower collector work function (ϕ_C), compared to a p-type one, can be obtained for the maximization of the thermionic output voltage, beyond the

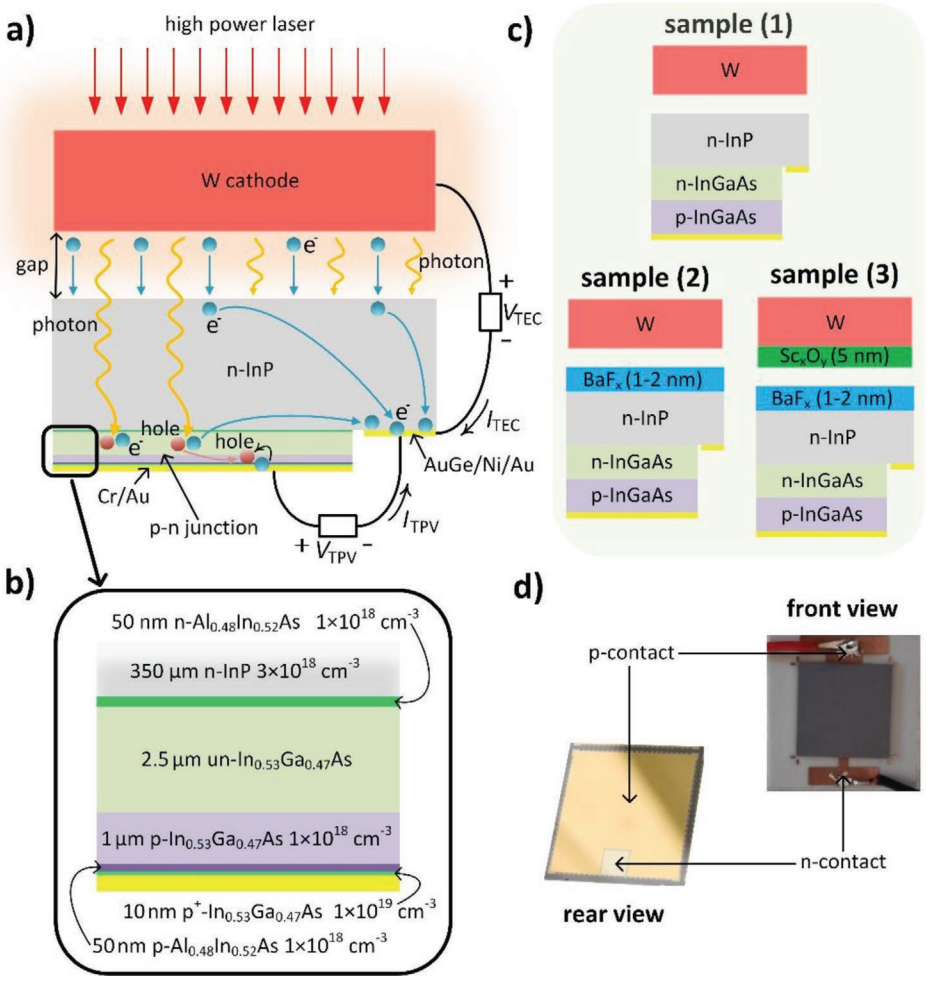

Figure 1. a) Three-terminal TIPV device comprising a tungsten (W) thermionic cathode and a PV/anode structure made of an n-InP anode and an InGaAs PV cell. Both thermionic and photogenerated carriers are collected independently through two rear contacts made in the monolithic PV/anode structure. Relatively few electron–hole pairs are generated in the InP substrate due to its large bandgap (1.34 eV), and most of them are produced and recombined near its front surface; thus, they do not contribute to the current of the device and are not shown in the figure; b) detailed semiconductor layer structure of the InGaAs PV cell; c) the three samples used in this work that use bare W and n-InP surfaces (sample 1) or incorporate different coatings on the anode (sample 2) and the cathode (sample 3); d) front and rear views of the fabricated PV/anode devices.

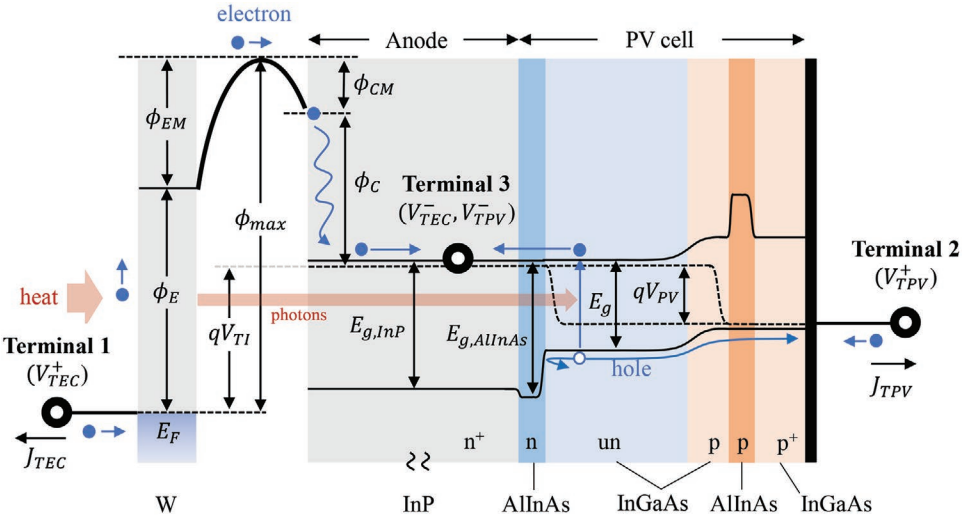

Figure 2. a) Band-diagram of the three-terminal TIPV converter made of a cathode/emitter (W) and a closely spaced PV/anode structure comprising a n-InP anode ($E_{g,InP}$ = 1.34 eV) and a PV cell made of InGaAs absorbing layer (E_g = 0.75 eV) and AlInAs window layers ($E_{g,AlInAs}$ = 1.47 eV). Electrons are injected through terminals 1 and 2, then pumped to a higher energy level by thermionic (terminal 1) and photovoltaic (terminal 2) effects, and finally extracted through terminal 3. The output voltages are the ones established between terminals 1 and 3 (V_{TI}, TEC contribution) and terminals 2 and 3 (V_{PV}, PV contribution). A small local separation of the quasi-Fermi energy levels is expected to take place within a small region in the InP layer due to the absorption of high energy photons. As this will not impact the device operation, they are not shown for the sake of simplicity.

possibility of surface coatings to further reduce the emitter and collector work functions (ϕ_E and ϕ_C, respectively). Moreover, thermionic and PV currents are extracted separately using two independent electrodes, one for electrons (both thermionic and photogenerated, that is, terminal 3 in Figure 2) and the other for holes (photogenerated, that is, terminal 2 in Figure 2). As a result, current is injected from terminal 3 (the anode) and extracted from terminals 1 and 2 (the cathodes). This avoids the current-matching constraint of the two-terminal configuration and allows independent biasing of each sub-device, resulting in the optimization of the maximum power extracted from each subcell regardless of a varying operating condition. The three-terminal TIPV concept also enables a higher power output throughout a wider temperature range,[9] making it more flexible than the two-terminal one when the external conditions, such as the operating temperature, vary. The difficulty in cell interconnection inherently arising under this scheme is related to the need for either two independent external circuits or some sophisticated electrical scheme for reconverting it into a two-terminal array, such as the one proposed by Gee.[14]

The possibility to discriminate the contribution from each (PV or TEC) process, assessing currents and voltages separately, is also of particular importance at this very early stage of the TIPV concept validation. Since both subcells work independently and, in principle, should be electrically decoupled from each other, a different output voltage is also obtained from each one. Indeed, the verification of the possible subcell cross-talking is a relevant feature to evaluate regarding this three-terminal TIPV implementation.

This article reports the first proof of concept demonstration of a three-terminal TIPV converter comprising a tungsten emitter (from now on referred to as "cathode") and a PV/anode structure made of an n-InP anode and an InGaAs interdigitated back contact (IBC) PV cell. We demonstrate a maximum power generation capacity of 125.6 and 0.35 mW cm^{-2} for the PV and thermionic sub-devices, respectively, operating at 1400 °C. We also demonstrate the capability of boosting the thermionic power by implementing low work function thermionic coatings without affecting the PV performance.

2. Methodology

The workflow for the fabrication of the PV/anode structures starts by optimizing doping and thickness of the epitaxial layer structure with PC1D,[15] resulting in the monolithic semiconductor layer architecture shown in Figure 1b. The simulations suggest an $In_{0.53}Ga_{0.47}As$ (E_g = 0.75 eV) p-type region as thin as possible and the minimum possible n-type region doping. However, a very conservative design was implemented were the p-type region thickness is kept at 1 µm, followed by an undoped 2.5 µm thick region. A highly doped (1×10^{19} cm^{-3}) and very thin (10 nm) $In_{0.53}Ga_{0.47}As$ contact layer is incorporated for implementing the external ohmic contact using a Cr/Au metallization. The n-type contact is made of AuGe/Ni/Au, which is annealed during 210 s at 410 °C to improve its specific contact resistance. Relatively high-bandgap $Al_{0.48}In_{0.52}As$ ternary alloys (E_g = 1.47 eV) are epitaxially grown lattice-matched to $In_{0.53}Ga_{0.47}As$ as back surface field (BSF) and window layers, to reduce surface recombination. These materials were selected targeting maximum absorption in the active layers (low bandgap $In_{0.53}Ga_{0.47}As$) and minimum absorption in the thermionic collector, window, and BSF layers (high bandgap $Al_{0.48}In_{0.52}As$ and InP). The epitaxial structure was manufactured by Xiamen Powerway Advanced Materials Co. Ltd. (China) using molecular beam epitaxy on a 2-inch InP substrate (E_g = 1.34 eV).

The structures were subsequently processed into devices following standard photolithographic techniques, including

selective chemical etching and thermal evaporation of metals. The IBC grid design is optimized using a quasi-3D distributed model,[16] fed with semi-empirical electronic parameters, and solved by SPICE (further details can be found on the Supporting Information). As a result, a configuration without alternating metal fingers corresponding to each contact, but with a continuous rear metallization covering most of the p-type contact and an n-type contact as small as possible is implemented instead (see Figure 1d). Such cell architecture, here called fingerless, makes advantage of the InP substrate for lateral transport of electrons toward the small intermediate n-type contact, while holes are vertically transported through the junction until they reach the spread-out rear p-contact metal. Large-area 1 cm^2 fingerless IBC PV/anode devices are processed and isolated by chemical mesa etching, they are diced, flipped (exposing the InP substrate upward), and finally encapsulated on insulated metal substrates using a low temperature soldering paste and cabled as shown in Figure 1d (see also Supporting Information).

Ultra-thin BaF_x and Sc_xO_y coatings are deposited by electron-beam evaporation (base pressure $< 4.0 \times 10^{-7}$ mbar) on the anode and cathode, respectively, to reduce the electrodes' work function, ultimately resulting in the three device configurations illustrated in Figure 1c. During the deposition process, the beam accelerating voltage and current were fixed to 8.3 kV × 65 mA and 6.7 kV × 10 mA for Sc_2O_3 (powder, 99.999% purity, W crucible) and BaF_2 (pellets, 99.9% purity, Cu crucible), respectively, maintaining the deposition rate at 0.04 nm s^{-1} constant during the process (operative pressure of $5.0 \pm 2.5 \times 10^{-6}$ mbar). An in situ quartz microbalance, connected automatically to a shutter valve, was used for monitoring the coating deposition rate, and finely controlling the desired thicknesses. The thickness of the films is established to be from 1 to 2 nm (70% estimated surface coverage) for BaF_x, which was found to induce a work function minimization for III–V semiconductor substrates down to 2.1 eV.[17] Sc_xO_y coatings with thickness of 5 nm was deposited on W cathodes, showing a stoichiometry close to the nominal one, stability in temperature, and a work function of 3.5 eV measured by UV photo-electron spectroscopy.

Before conducting the high temperature thermionic emission experiments, the absolute external quantum efficiency (EQE) of the PV/anode devices has been measured with a lock-in amplifier equipped with a transimpedance pre-amplifier under illumination of a quartz tungsten halogen lamp coupled with a grating monochromator equipped with order sorting filters. The current density-to-voltage *J–V* curves have been measured as a function of the illumination intensity using a Xe lamp multi-flash solar simulator[18].

The high temperature TIPV device characterization is carried out in an ultrahigh vacuum condition (base pressure 7.5×10^{-8} mbar). The PV/anode is mounted on a holder that is cooled at 5 °C (using water plus 20% of glycol ethylene). The PV/anode holder temperature is continuously monitored by a type-K thermocouple. The two circuits of the three-terminal TIPV device are biased/measured with a Keithley source-meter (mod. 2470) using a four-wire configuration, although two-wires configuration provided the same results. The polycrystalline W cathode is heated up by illuminating its rear side with a focused continuous laser diode (818 nm wavelength, maximum 230 W optical power) and its temperature is monitored using a type-C thermocouple, a Minolta Cyclopes 152 pyrometer, and an IR thermal camera through a ZnSe viewport of the chamber. The two electrodes are approached using a movement system composed by a continuous DC motor and an incremental optical encoder system to move the PV/anode toward the cathode, with a resolution of 0.5 µm. A large inter-electrode distance of 125 ± 20 µm has been established to avoid planarity issues which could occur at gaps smaller than 100 µm, finding the selected value as the best compromise between the avoidance of possible contacts between the electrodes which can cause PV/anode structure degradation due to thermal expansions at ultra-high temperature and minimization of the effects of larger gaps on the electron emission/collection mechanism.

3. Experimental Results

Figure 3 shows the electric output characteristics of a three-terminal TIPV converter operating at different cathode temperatures and with different anode and cathode surface terminations: 1) bare n-InP and W, 2) BaF_x:InP and bare W, and 3) BaF_x:InP and Sc_xO_y:W (see Figure 1c). Figure 3a,b shows the *I–V* characteristics of the PV and TEC sub-devices respectively, whereas Figure 3c,d shows the thermionic saturation current and the output power density, respectively, as a function of the cathode temperature.

It has been experimentally corroborated that the *I–V* curves of the PV sub-device (Figure 3a) are not affected by the different anode and cathode terminations neither by the different bias conditions of the thermionic sub-device. The former is attributed to the very thin coatings (5 nm of Sc_xO_y on the cathode, 1–2 nm of BaF_x on the anode) that do not modify the optical properties, but only the electronic properties of their surfaces. The EQE of the PV sub-device is shown in **Figure 4**a along with the spectral irradiance of tungsten, calculated using tabulated data for tungsten emissivity as in ref. [12]. It shows a response between 70% and 80% in the whole absorption range, from 0.73 to 1.34 eV, which is a high value, considering that the cell does not have any anti-reflection coating. The InP substrate absorption cancels the EQE signature over 1.34 eV, which is the InP bandgap at room temperature, but this is acceptable, as spectral irradiance from the cathode is low at such high photon energies. Figure 4b shows the calculated current density (blue solid line), obtained by integrating the EQE with the spectral irradiance of tungsten and considering a view factor of 0.61, which is needed to match the current density measured during the high temperature characterization of TIPV devices (blue squares). *J–V* curves under high intensity illumination using a flash simulator were measured up to a PV cell short circuit current of 2.2 Acm^{-2} and the fit to the open-circuit voltage (V_{OC}) that is obtained from these measurements is shown as the solid red line in Figure 4b. The short pulses of the flash simulator prevent cell overheating ensuring cell is at room temperature. The V_{OC} with the cell at room temperature measured using the flash simulator equals the one measured during the high temperature TIPV characterization at low cathode temperatures (≈850 °C) implying the cell does not overheat at this temperature during its characterization as TIPV device. However, at

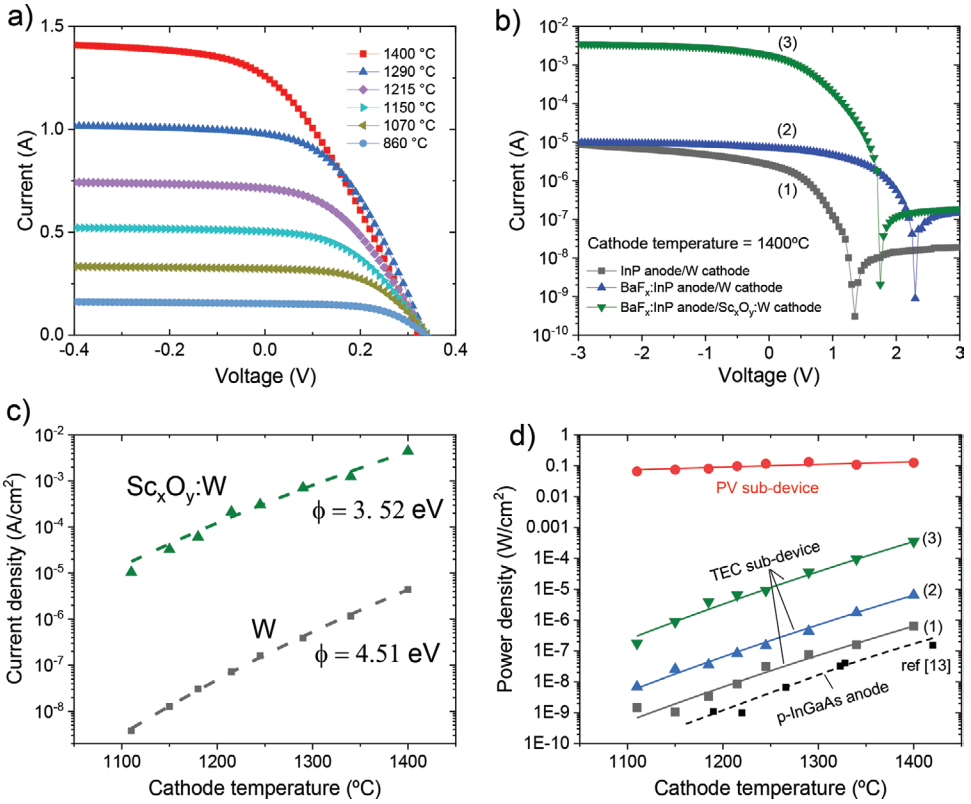

Figure 3. Output electrical characteristics of the three-terminal TIPV converter. a)The *I–V* curves of the PV sub-device as a function of the cathode temperature. Different electrodes' coatings and different bias conditions of the TEC sub-device do not induce any modifications of such curves. b) The *I–V* curves (current is in absolute value) of the three kinds of thermionic sub-devices, depending on the surface coating on the anode and the cathode. c)The forward saturation current density for the two cathodes used in this work, namely Sc_xO_y:W and bare W. The work function values that are obtained for each case from the fitting to the Richardson–Dushman equation are shown. d) The output power density of PV and the three thermionic sub-devices (using the three kinds of samples indicated in Figure 1c) along with the one reported in our previous work using (non-PV) p-InGaAs anodes.[13]

higher temperatures, the V_{OC} under TIPV experimental conditions is considerably lower due to cell overheating. Experimentally, only the temperature of the PV/anode holder could be measured, and thus, the temperature of the PV cell semiconductor layers is unknown. However, previous theoretical studies suggest that a high thermal gradient exists along the thickness of the PV/anode architecture,[19] thus the cell overheating is likely to occur. Assuming a change in the V_{OC} of 1.6 mV °C^{-1} for InGaAs PV cells at 1.5 A cm^{-2} short-circuit current conditions,[20] which agrees with our own observations in InGaAs PV devices, results indicate that the junction overheats up to ≈50 °C over room temperature at a cathode temperature of 1400 °C.

Three different thermionic sub-device output characteristics are shown in Figure 3b depending on the cathode and

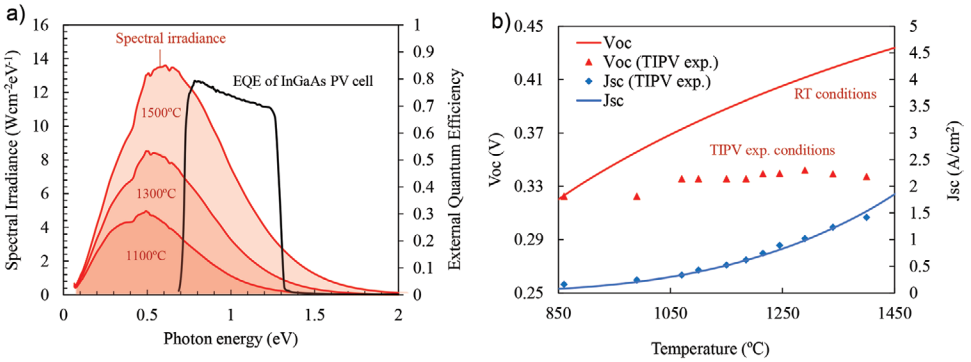

Figure 4. a) Experimental EQE of the InGaAs PV/anode structure and the calculated spectral irradiance of tungsten, obtained using tabulated data for tungsten emissivity as in ref. [12]; b) open-circuit voltage and short-circuit current density of the PV/anode device as a function of the cathode temperature. The solid line for the short-circuit current is obtained by integrating the EQE with the spectral irradiance of tungsten and considering a view factor of 0.61. The solid lines for the open-circuit voltage represent the interpolation of the experimental value measured under high intensity illumination at room temperature.

anode surface terminations (as indicated in Figure 1c). In all the cases, forward saturation current (measured at large negative voltages) is higher than backward saturation current (measured at large positive voltages) due to the higher temperature of the cathode. Large voltages (V_{TI} in Figure 2) accelerate electrons from the cathode to the anode (if negative) and from the anode to the cathode (if positive), resulting in an increase of the thermionic current until it reaches a saturated value, which is determined by the maximum number of electrons that can be emitted from each surface. Due to the electron acceleration, the saturation currents are not affected by possible interelectrode space-charge energy barriers (i.e., ϕ_{CM} and ϕ_{EM} in Figure 2), and they are solely determined by the surface properties (e.g., surface work functions ϕ_C and ϕ_E, Richardson constant, etc.) and their temperature. This explains why samples with the same cathode termination (1 and 2) have identical forward saturation current, whereas samples with the same anode termination (2 and 3) have identical backward saturation current. Moreover, the higher backward saturation current of samples 2 and 3 than that of sample 1 is attributed to the lower work function of the anode (BaF_x:InP), whereas the higher forward saturation current of sample 3 (compared to samples 1 and 2) is attributed to the lower work function of the cathode (Sc_xO_y:W). The work function of W and Sc_xO_y:W cathodes is estimated to be 4.5 and 3.5 eV, respectively, from the fit of the Richardson–Dushman model, that is, $AT^2\exp(-\phi/kT)$ (being A the Richardson–Dushman constant of the emitting material, T the cathode temperature, ϕ the work function, and k the Boltzmann constant) to the experimental forward saturation current measured as a function of the cathode temperature (Figure 3c).

The largest differences between the three thermionic subdevices compared here are observed in the power generation quadrant, where voltages and currents are positive and the electrons flow against the electric field established within the interelectrode gap. In this region, the V_{OC} represents the limiting condition where forward and backward currents are indentical, and can be approximated by the voltage that produces the minimum currents shown for each sample (in absolute value) in Figure 3b. In these conditions, and according to the Langmuir's space-charge theory,[21] the very low net currents preclude the creation of a space charge, and subsequently, the V_{OC} is solely determined by the surface properties of the cathode and the anode, mainly the difference between their work functions. Thus, according to this theory, the highest V_{OC} that is measured in sample 2 is attributed to the largest difference between the cathode/emitter (W, ϕ_E = 4.5 eV) and the anode/collector (BaF_x:InP, ϕ_C = 2.1 eV) work functions. Similarly, the smallest V_{OC} that is obtained for sample 1 is attributed to the smallest difference between the cathode (W, ϕ_E = 4.5 eV) and the anode (InP, ϕ_C = 3.7 eV) work functions. In sample 3, the difference between the cathode (Sc_xO_y:W, ϕ_E = 3.5 eV) and the anode (BaF_x:InP, ϕ_C = 2.1 eV) work function is in between the other two, and thus, it produces an intermediate V_{OC} (≈0.4 eV less than for bare W cathode). Nevertheless, the much higher saturation current of sample 3, if compared to samples 1 and 2, results is a much higher output power, regardless of the lower output voltage.

The resulting output power density of both PV and TEC subdevices is shown as a function of the cathode temperature in Figure 3d, which illustrates the relative improvements on the thermionic sub-device performance by reducing the work function of the cathode and the anode. First, sample 1 produces a higher thermionic output power than the one obtained in our recent work[13] by simply using n-InP rather than p-InGaAs for the anode. This is attributed to the lower workfunction of n-InP than p-InGaAs, as explained before. Figure S2, Supporting Information shows that V_{OC} of the n-InP thermionic converter is higher than that of the p-InGaAs one, which reinforces this conclusion. Moreover, Figure S3, Supporting Information shows that the thermionic sub-device reported in this work (sample 1) produces more power than the complete 2-terminal TIPV device reported previously in ref. [13], meaning that the PV voltage boost of the 2-terminal device is not enough to offset the higher anode workfunction. Second, further reducing the work function of the anode (samples 2 and 3) and the cathode (sample 3) results in an additional increment of the thermionic power. This is attributed to an increase in the output voltage (samples 2 and 3) and the output current (sample 3), as explained above. This increase in the power density indicates that TIPV performance can be improved by surface engineering of the anode. This is a promising result for the future research in TIPV converters, pushing toward the development of thermionic coatings with much lower work function and higher Richardson constant to bring the thermionic sub-device output power to the range of that of PV sub-device.

4. Conclusions

In summary, we have demonstrated a three-terminal hybrid thermionic-PV converter that solves the current-matching issues of two-terminal configurations, and thus, it is able to discriminate the thermionic and PV power contributions. The device uses a PV/anode structure with two independent electrodes developed in the rear surface, one for collecting the electrons (thermionic and PV) and the other for collecting the holes (PV). When the cathode is heated at 1400 °C the PV sub-device produces 125.6 mW cm^{-2}, whereas the thermionic sub-device produces 0.35 mW cm^{-2}. This result has been obtained using a W cathode covered by 5 nm of Sc_xO_y (work function of 3.5 eV) and an n-type InP anode, including an InGaAs PV cell, covered by 1–2 nm of BaF_x (work function of 2.1 eV), and an inter-electrode gap of 125 μm. The relatively high work function coatings and the large interelectrode gaps used in this work preclude achieving a high thermionic power contribution. However, power densities around 1 W cm^{-2} have been obtained by TECs with interelectrode gaps ≤ 10 μm.[3,22–24] In this context, these experimental results indicate that the power generated by the PV sub-device is significant and will therefore contribute to increase output power and conversion efficiency of optimized future TECs. Besides, the PV contribution is expected to rise when the interelectrode distances are reduced to the micro/nanoscale, which is necessary to address the space-charge issues of thermionic energy conversion, and the near-field thermal radiation becomes significant. Thus, future work should focus on developing micro/nanoscale device configurations that incorporate ultralow workfunction coatings to ultimately enable a highly efficient hybrid thermionic-PV power generation that overcomes the limitations of independent TPV and TEC devices.

Supporting Information

Supporting Information is available from the Wiley Online Library or from the author.

Acknowledgements

This work was partially funded by the European FET-OPEN project AMADEUS (Grant agreement no. 737054); the project Termocell (ENE2017-86683-R) funded by the Ministerio de Economía, Industria y Competitividad; the project GeTPV (PID2020-115719RB-C22) funded by the Ministerio de Ciencia e Innovación and by the projects ANDREA (M190020074ADM, "programa de apoyo a la realización de Proyectos de I+D para jóvenes investigadores 2019") and MADRID-PV2 (S2018/EMT-4308) funded by the Comunidad de Madrid with support from European Regional Development Fund (ERDF/FEDER).

Conflict of Interest

The authors declare no conflict of interest.

Author Contributions

A.B. and P.G.L. contributed equally to this work. Conceptualization: A.D.; methodology: A.B., P.G.L., A.M., D.M.T., and A.D.; formal analysis: A.B., A.D.; investigation: A.B., P.G.L.; writing—original draft: A.D., P.G.L.; writing—review and editing: A.B., P.G.L, A.M, D.M.T., and A.D.; supervision: A.D. A.M., and D.M.T.; project administration: A.D. A.M., and D.M.T.; funding acquisition: A.D., A.M., P.G.L., and D.M.T.

Data Availability Statement

The data that support the findings of this study are available from the corresponding author upon reasonable request.

Keywords

InGaAs, InP, interdigitated back contacts, photovoltaics, thermionics, thermophotovoltaics, three-terminal

Received: January 28, 2022
Revised: March 8, 2022
Published online: April 11, 2022

[1] T. Burger, C. Sempere, B. Roy-Layinde, A. Lenert, *Joule* **2020**, *4*, 1660.
[2] A. Datas, R. Vaillon, in *Ultra-High Temperature Thermal Energy Storage, Transfer and Conversion*, (Ed.: A. Datas), Woodhead Publishing, Sawston **2021**, pp. 285–308.
[3] M. F. Campbell, T. J. Celenza, F. Schmitt, J. W. Schwede, I. Bargatin, *Adv. Sci.* **2021**, *8*, 2003812,
[4] D. M. Trucchi, A. Bellucci, M. Girolami, P. Calvani, E. Cappelli, S. Orlando, R. Polini, L. Silvestroni, D. Sciti, A. Kribus, *Adv. Energy Mater.* **2018**, *8*, 1802310,
[5] D. Fan, T. Burger, S. Mcsherry, B. Lee, A. Lenert, S. R. Forrest, *Nature* **2020**, *586*, 237,
[6] Z. Omair, G. Scranton, L. M. Pazos-Outón, T. P Xiao, M A. Steiner, V. Ganapati, P. F. Peterson, J. Holzrichter, H. Atwater, E. Yablonovitch, *Proc. Natl. Acad. Sci. USA* **2019**, *116*, 15356,
[7] W. Liu, Q. Jie, H. S. Kim, Z. Ren, *Acta Mater.* **2015**, *87*, 357,
[8] J.-H. Lee, I. Bargatin, N. A. Melosh, R. T. Howe, *Appl. Phys. Lett.* **2012**, *100*, 173904,
[9] A. Datas, *Appl. Phys. Lett.* **2016**, *108*, 143503,
[10] A. Datas, R. Vaillon, *Appl. Phys. Lett.* **2019**, *114*, 133501,
[11] A. Datas, R. Vaillon, *Nano Energy* **2019**, *61*, 10,
[12] A. Bellucci, M. Mastellone, V. Serpente, M. Girolami, S. Kaciulis, A. Mezzi, D. M. Trucchi, E. Antolín, J. Villa, P. G. Linares, A. Martí, A. Datas, *ACS Energy Lett.* **2020**, *5*, 1364.
[13] A. Bellucci, P. G. Linares, J. Villa, A. Martí, A. Datas, D. M. Trucchi, *Sol. Energy Mater. Sol. Cells* **2022**, *238*, 111588,
[14] J. M. Gee, *Sol. Cells* **1988**, *24*, 147,
[15] P. A. Basore, D. T. Rover, A. W. Smith, in *Conf. Record of the 20th IEEE Photovoltaic Specialists Conf*, IEEE, Piscataway **1988**, pp. 389–396.
[16] I. Garcia, C. Algora, I. Rey-Stolle, B. Galiana, in *2008 33rd IEEE Photovoltaic Specialists Conf*, IEEE, Piscataway **2008**, pp. 1–6.
[17] V. Serpente, A. Bellucci, M. Girolami, M. Mastellone, A. Mezzi, S. Kaciulis, R. Carducci, R. Polini, V. Valentini, D. M. Trucchi, *Mater. Chem. Phys.* **2020**, *249*, 122989,
[18] C. Domínguez, P. Garcia-Linares, in *High Concentrator Photovoltaics – Fundamentals, Engineering and Power Plants*, Springer International Publishing, New York **2015**, pp. 39–84.
[19] M. Zeneli, A. Bellucci, G. Sabbatella, D. M. Trucchi, A. Nikolopoulos, N. Nikolopoulos, S. Karellas, E. Kakaras, *Energy Convers. Manag.* **2020**, *210*, 112717,
[20] D. M. Wilt, N. S. Fatemi, R. W. Hoffman, P. P. Jenkins, *AIP Conf. Proc.* **1995**, *321*, 210,
[21] G. N. Hatsopoulos, E. P. Gyftopoulos, *Thermionic Energy Conversion*, The MIT Press, Cambridge **1979**.
[22] M. F. Campbell, M. Azadi, Z. Lu, A. G. Eskenazi, A. Jain, J. W. Bang, P. G. Sieg, G. A. Popov, S. M. Nicaise, K. C. Van Houten, F. Schmitt, J. W. Schwede, I. Bargatin, *J. Microelectromech. Syst.* **2020**, *29*, 637,
[23] G. Hatsopoulos, J. Kaye, *Proc. IRE* **1958**, *46*, 1574,
[24] J. E. Beggs, *Adv. Energy Convers.* **1963**, *3*, 447,